EUROPEAN ORGANIZATION FOR NUCLEAR RESEARCH

CERN-EP/2002-065
August 2, 2002

Search for Single Top Production at LEP

The L3 Collaboration

Abstract

Single top production in e^+e^-annihilations is searched for in data collected by the L3 detector at centre-of-mass energies from 189 to 209 GeV, corresponding to a total integrated luminosity of 634 pb^{-1}. Investigating hadronic and semileptonic top decays, no evidence of single top production at LEP is obtained and upper limits on the single top cross section as a function of the centre-of-mass energy are derived. Limits on possible anomalous couplings, as well as on the scale of contact interactions responsible for single top production are determined.

Submitted to *Phys. Lett. B*

Introduction

One of the fundamental features of the Standard Model is that neutral currents are flavour diagonal, therefore any flavour changing neutral current (FCNC) process may occur only at second or higher orders through loops. The FCNC interactions of the top quark offer an ideal place to search for new physics and can be studied either in $\mathrm{t} \rightarrow \mathrm{qV}$ ($\mathrm{q} = \mathrm{u}, \mathrm{c}$; $\mathrm{V} = \gamma, \mathrm{Z}$) decays at the Tevatron or in single top production at LEP. In the Standard Model, the predicted rates of such processes are very small [1], but new physics beyond the Standard Model could lead to a significant increase. Enhancements of some orders of magnitude are predicted in two-Higgs-doublet models and supersymmetric models [2]. Flavour changing multiple-Higgs-doublet models further enhance the rates up to 10^{-5} [3], and models with FCNC coupled singlet quarks, compositeness or dynamical electroweak symmetry breaking [4] can yield a branching ratio of about 10^{-2}, in the reach of present colliders. The same considerations apply for the predicted single top production rates [5]. Experimental upper limits at the 95% confidence level on the FCNC branching fractions of the top quark were set by the CDF Collaboration as $\mathrm{BR}(\mathrm{t} \rightarrow \mathrm{c(u)}\gamma) < 3.2\%$ and $\mathrm{BR}(\mathrm{t} \rightarrow \mathrm{c(u)Z}) < 33\%$ [6]. Other studies of single top production were carried out at LEP [7].

In this Letter, we consider two theoretical models for single top production $\mathrm{e}^+\mathrm{e}^- \rightarrow \mathrm{t}\bar{\mathrm{c}}$ [1)]: an interpretation involving $[\mathrm{t}\bar{\mathrm{c}}\mathrm{e}^+\mathrm{e}^-]$ contact interactions and an approach which describes the process in terms of anomalous couplings.

Single Top Production through Contact Interactions

An effective flavour changing vertex can be parameterized through $[\mathrm{t}\bar{\mathrm{c}}\mathrm{e}^+\mathrm{e}^-]$ contact interactions [8]. The total unpolarised cross sections for $\mathrm{e}^+\mathrm{e}^- \rightarrow \mathrm{t}\bar{\mathrm{c}}$ and charge conjugate can be written as:

$$\sigma = \mathcal{C}\left[(3+\beta)(V_{LL}^2 + V_{RR}^2 + V_{RL}^2 + V_{LR}^2) + \frac{3}{2}(1+\beta)S_{RR}^2 + 8(3-\beta)T_{RR}^2\right] \tag{1}$$

where V_{ij}, S_{ij}, T_{ij} represent the coupling constants of vector, scalar and tensor fields, respectively (L and R stand for left-handed and right-handed fields), $\mathcal{C} = s/\Lambda^4 \times \beta^2/4\pi(1+\beta)^3$, $\beta = (s - m_\mathrm{t}^2)/(s + m_\mathrm{t}^2)$ and Λ is the energy scale parameter for the process. The predicted single top production cross sections are shown in Figure 1a for three different assumptions on the Lorentz structure of the $[\mathrm{t}\bar{\mathrm{c}}\mathrm{e}^+\mathrm{e}^-]$ vertex. In this Letter, we give lower limits on the energy scale Λ. No directly comparable previous limits exist.

Anomalous Couplings

The Born-level cross section for the single top production process $\mathrm{e}^+\mathrm{e}^- \rightarrow \mathrm{t}\bar{\mathrm{c}}$ in the presence of anomalous couplings $\mathrm{tV}\bar{\mathrm{c}}$, with $\mathrm{V} = \gamma, \mathrm{Z}$ [9, 10], is given by:

$$\sigma = \frac{\pi\alpha^2}{s}\Big(1-\mathcal{M}_\mathrm{t}\Big)^2\left[\frac{\kappa_\gamma^2 e_\mathrm{q}^2}{\mathcal{M}_\mathrm{t}}\Big(1+2\mathcal{M}_\mathrm{t}\Big) + \frac{\kappa_\mathrm{Z}^2(1+a_\mathrm{W}^2)(2+\mathcal{M}_\mathrm{t})}{4\mathcal{S}_\mathrm{W}^2(1-\mathcal{M}_\mathrm{Z})^2} + \frac{3\kappa_\mathrm{Z}\kappa_\gamma a_\mathrm{W} e_\mathrm{q}}{\mathcal{S}_\mathrm{W}(1-\mathcal{M}_\mathrm{Z})}\right] \tag{2}$$

in the limit of a massless c quark; κ_γ and κ_Z define the strength of the anomalous coupling for the current with a photon and a Z boson, respectively, s is the centre-of-mass energy squared, α is the fine structure constant, $e_\mathrm{q} = 2/3$ and m_t are the charge fraction and the mass of

[1)] Charge conjugate is assumed throughout this Letter.

the top quark, $a_W = 1 - 4\sin^2\theta_W$, $\mathcal{S}_W = \sin^2 2\theta_W$, θ_W is the Weinberg angle, $\mathcal{M}_t = m_t^2/s$ and $\mathcal{M}_Z = m_Z^2/s$. QCD corrections are taken into account following the prescriptions of Reference 11. Moreover, the effect of initial state radiation (ISR) must be included. Born-level and QCD+ISR corrected predictions for the cross section are shown in Figure 1b. The FCNC branching fraction limits set by CDF correspond to upper limits on the anomalous couplings of $\kappa_\gamma^2 < 0.176$ and $\kappa_Z^2 < 0.533$ [9], at the 95% confidence level.

Data and Monte Carlo Samples

This study is based on 634 pb^{-1} of data collected by the L3 detector [12] at LEP at $\sqrt{s} = 189 - 209$ GeV. This integrated luminosity corresponds to the seven ranges of average centre-of-mass energies shown in Table 1.

$<\sqrt{s}>$ (GeV)	188.6	191.6	195.5	199.6	201.8	204.8	206.6
Luminosity (pb^{-1})	176.8	29.8	84.1	84.0	37.7	86.0	135.5

Table 1: Average centre-of-mass energies and their corresponding integrated luminosities.

Crucial to this analysis is the prediction of Standard Model backgrounds, which rely on the following Monte Carlo (MC) programs: PYTHIA [13] and KK2f [14] for $e^+e^- \to q\bar{q}(\gamma)$, KORALW [15] for $e^+e^- \to W^+W^-$, KORALZ [16] for $e^+e^- \to \tau^+\tau^-$, PHOJET [17] for two-photon interactions and EXCALIBUR [18] for other four-fermion final states. Single top production MC events were generated with a modified version of PYTHIA [19]. QCD colour reconnection effects are taken into account in the framework of the Lund fragmentation model [20], forcing the top decay $t \to W^+b$ before the fragmentation takes place.

The response of the L3 detector is simulated using the GEANT [21] program, taking into account the effects of multiple scattering, energy loss and showering in the detector. Hadronic interactions in the detector are modeled using the GHEISHA [21] program. Time dependent detector inefficiencies, as monitored during the data taking period, are also simulated.

Analysis Procedures

In the reaction $e^+e^- \to t\bar{c}$ at LEP centre-of-mass energies, the top quark is produced almost at rest and quickly decays via $t \to W^+b$ without forming top-flavoured hadrons. Depending on the subsequent decay of the W boson, the expected final state signatures are two jets, one lepton and missing energy ($t\bar{c} \to W^+b\bar{c} \to l^+\nu b\bar{c}$) or four jets ($t\bar{c} \to W^+b\bar{c} \to q\bar{q}'b\bar{c}$), hereafter referred to as the leptonic and hadronic channels, respectively. In both channels, the c-quark energy E_c has a fixed value for a given $\sqrt{s}$:

$$E_c = \frac{\sqrt{s}}{2}\left(1 - \frac{m_t^2}{s}\right), \tag{3}$$

whereas the b-quark energy E_b has an almost fixed value which does not depend on $\sqrt{s}$, in the limit of a top quark at rest in the centre-of-mass frame:

$$E_b \simeq \frac{m_t}{2}\left(1 - \frac{m_W^2}{m_t^2}\right), \tag{4}$$

where $m_{\rm W}$ is the mass of the W boson. After hadronisation, the c and b quarks yield jets with almost fixed energies. Since both channels are characterised by the presence of a b quark, a clear signature exists and is exploited by using a b-jet tagging algorithm [22], which is mainly based on lifetime information.

Standard search procedures are applied to both the leptonic and hadronic channels. First, a preselection is applied which significantly reduces the background while keeping a high signal efficiency; this is especially effective against background from low multiplicity events and from two-photon interactions. Then, a further set of channel-specific selection criteria is chosen to increase the signal-to-background ratio. Finally, a discriminating variable is built using a neural network technique.

Leptonic Channel

The signature for the leptonic channel is one energetic lepton, large missing momentum and two jets with a large difference in energy. The most energetic jet is assumed to stem from the hadronisation of the b quark. The $\rm e^+e^- \rightarrow W^+W^-$ and $\rm e^+e^- \rightarrow q\overline{q}(\gamma)$ processes constitute the main background.

A preselection is applied requiring events to have at least three tracks, more than 15 calorimetric clusters and a visible energy greater than $0.25\times\sqrt{s}$, but less than $0.9\times\sqrt{s}$. The presence of a well identified lepton is required; if there is more than one reconstructed lepton, the most energetic one is retained. An electron candidate is identified as a track with an associated cluster in the electromagnetic calorimeter; a muon candidate is reconstructed as a track in the central tracker matched to one in the muon spectrometer; a tau lepton is identified as a low-multiplicity jet. All clusters in the event, except the ones associated with the reconstructed lepton, are combined to form two hadronic jets using the DURHAM algorithm [23]. The jet axes and the missing momentum vector must be at least 15° and 26°, respectively, away from the beam axis.

To further reject background events, the energy of the lepton is required to be at least 10 GeV. The energy of the most energetic jet is required to exceed 60 GeV, whereas an upper bound is set on the energy E_1 of the least energetic jet, as detailed in Table 2. The width of the least energetic jet must be less than 0.4, the jet width being defined as the scalar sum of the transverse momenta of the jet clusters, normalised to the jet energy. The missing momentum is required to exceed 25 GeV, the lepton plus missing momentum invariant mass must be larger than 20 GeV and the two-jet invariant mass $M_{\rm q\overline{q}}$ has to lie outside a window around the W mass, as given in Table 2. The distributions of some relevant variables are shown in Figure 2. From the overall selection, 346 events are left in the data sample, with 357.0 ± 1.8 expected from Standard Model backgrounds. The signal efficiency is 10.6% as detailed in Table 3 which also gives results at all centre-of-mass energies. In order to enhance the separation between signal and background, a neural network technique [24] is then employed. The most important event variables are used as inputs to a neural network with 10 input nodes and two output

$\sqrt{s}$ (GeV)	188.6	191.6	195.5	199.6	201.8	204.8	206.6
E_1 (GeV) $\leq$	17.0	21.0	23.0	27.0	30.0	34.0	34.0
$\lvert M_{\rm q\overline{q}} - m_{\rm W}\rvert$ (GeV) $\geq$	14.0	11.0	8.5	6.0	6.0	3.0	3.0

Table 2: Centre-of-mass energy dependent cuts used for the leptonic channel.

nodes, $\mathcal{O}_{tc}$, $\mathcal{O}_{back}$, corresponding to the signal and the background, respectively. The input variables are related to the magnitude and direction of the missing momentum vector, the b-tag value, the invariant mass of the two-jets system and the invariant mass of the lepton plus missing-momentum system. The final discriminating variable is then obtained as the product $\mathcal{O} = \mathcal{O}_{tc} \times (1 - \mathcal{O}_{back})$.

	Leptonic channel			Hadronic channel		
$\sqrt{s}$ (GeV)	Data	Back.	Sig. eff. (%)	Data	Back.	Sig. eff. (%)
188.6	10	13.6 ± 0.3	10.7 ± 0.2	95	76.6 ± 0.8	21.0 ± 0.4
191.6	3	4.6 ± 0.2	11.1 ± 0.3	14	14.3 ± 0.5	23.1 ± 0.6
195.5	23	21.1 ± 0.4	10.4 ± 0.3	43	38.7 ± 1.0	22.1 ± 0.6
199.6	35	40.5 ± 0.4	10.7 ± 0.3	37	38.1 ± 0.5	21.5 ± 0.6
201.8	22	23.7 ± 0.2	10.2 ± 0.3	19	19.4 ± 0.4	21.6 ± 0.6
204.8	104	99.1 ± 1.1	10.5 ± 0.3	50	41.1 ± 0.7	20.7 ± 0.6
206.6	149	154.4 ± 0.9	10.5 ± 0.3	63	59.7 ± 0.6	20.2 ± 0.5
All	346	357.0 ± 1.8	10.6 ± 0.1	321	287.9 ± 1.6	21.1 ± 0.2

Table 3: The number of data events for each centre-of-mass energy range, the expected number of background events and the Monte Carlo predicted signal efficiencies, for both the leptonic and hadronic channels. The errors are statistical only. The signal efficiency is for a top quark mass of 175 GeV. The corresponding W decay branching fraction is taken into account in the signal efficiency.

Hadronic Channel

The signature for the hadronic channel is four hadronic jets, two jets having an almost fixed energy and two being the decay products of a W. In addition, one jet must have a strong b-jet signature. The $e^+e^- \to W^+W^-$ and $e^+e^- \to q\bar{q}(\gamma)$ processes constitute the main background.

A hadronic preselection, which requires a visible energy of at least $0.7 \times \sqrt{s}$ and an effective centre-of-mass energy larger than $0.85 \times \sqrt{s}$, is applied. The effective centre-of-mass energy is computed after having removed photon radiation in the initial state. We also require more than 20 reconstructed tracks and more than two jets, built using the DURHAM algorithm with a resolution parameter $y_{cut} = 0.02$.

The events are forced into a four-jet topology by changing the value of y_{cut}. The c-jet candidate is defined as the jet whose energy is closest to the value expected from Equation (3) for $m_{\mathrm{t}} = 174.3$ GeV. Using the remaining three jets, the W boson is identified as the jet pair with invariant mass closest to the nominal W mass. The remaining jet is assumed to be the b jet.

By comparing the direction of the leading c quark in MC events with the c-jet defined above, it is observed that the c selection purities are about 49%, 53% and 60% for $\sqrt{s} = 186.6$, 191.6 and 195.5 GeV, respectively, and approach the limit of 62% for $\sqrt{s} \geq 201.8$ GeV.

A neural network with 24 input nodes and three output nodes is then used. The neural network input variables are related to such jet characteristics as their energies and masses, the b-tag discriminant of the b jet candidate and various event shape variables. Some of these distributions are shown in Figures 3a and 3b. One network output selects the signal and is used as the final discriminating variable. The other two outputs, which tag $e^+e^- \to q\overline{q}(\gamma)$ and $e^+e^- \to W^+W^-$ events, are used to further reject the background by applying a cut of 0.1 and 0.3, respectively. Their distributions are shown in Figures 3c and 3d. After all cuts, the final sample consists of 321 data events, to be compared with 287.9 ± 1.6 expected background events, and a 21.1% signal efficiency, as detailed in Table 3.

Study of Systematic Uncertainties

The search for single top production discussed in this Letter relies heavily on the comparison between the data and its associated Monte Carlo simulations. Uncertainties in these simulations give rise to three sources of systematic uncertainties whose effects on the single top cross section are shown in Table 4. First, the finite statistics of the Monte Carlo used for the signal and background simulations affect the determination of the signal efficiency and the level of background contamination. Secondly, the background cross sections are fixed in the interpretation of the observed events in terms of the single top cross section. The effects of a variation of the $e^+e^- \to q\overline{q}(\gamma)$, $e^+e^- \to W^+W^-$ and $e^+e^- \to ZZ$ cross sections of 2%, 0.5% and 10%, respectively, are reported in Table 4. Thirdly, there can be differences between the actual and simulated detector performance, affecting the description of variables used as inputs to the neural network. In particular, we study the variables used for the lepton identification, the global event shape, the energy measurement and the b-tag. Their effects on the single top cross section are also given in Table 4, that also lists effects from the modeling of other variables. Finally, the systematic due to uncertainties in the measurement of the integrated luminosity is negligible.

Source	$\Delta\sigma/\sigma$ (%)
MC background statistics	0.4
MC signal statistics	1.7
$e^+e^- \to q\overline{q}(\gamma)$ modeling	0.2
$e^+e^- \to W^+W^-$ modeling	$<$ 0.1
$e^+e^- \to ZZ$ modeling	0.4
Lepton identification	0.1
Event shape	0.9
Energy resolution	1.6
b-tagging	1.4
Other variables	0.5
Luminosity	$<$ 0.1
Signal angular distribution	2.0

Table 4: Relative systematic uncertainties affecting the single top cross section.

In addition to these effects, uncertainties in the modeling of the signal process can affect our results. To quantify this, various signal samples with different final-state angular distributions are simulated, inside the limits allowed by the anomalous coupling scenario, with the effects reported in Table 4. An additional source of uncertainty could be the value of m_t used in the simulation. The low momenta available for the top system at our centre-of-mass energies would imply a change in the event kinematics and hence in the selection efficiency. Rather than assigning a systematic uncertainty from this source, all results are parametrised in terms of m_{t}.

Results

Leptonic and hadronic final discriminating variables are shown in Figure 4. A very good discrimination between signal and background is achieved. No significant deviation from the Standard Model background expectation is observed. Combined 95% confidence level upper limits on the single top total cross section are derived [25] and listed in Table 5. For these limits, the branching ratio for the top decay is assumed to be saturated by $\mathrm{t} \rightarrow \mathrm{Wb}$. The limits are obtained for the signal process $\mathrm{e^+e^-} \rightarrow \mathrm{t\bar{c}}$, a deterioration of the limits of about 10% is found for the corresponding process $\mathrm{e^+e^-} \rightarrow \mathrm{t\bar{u}}$.

Table 6 lists the 95% confidence level lower limit on the energy scale parameter Λ of a possible $[\mathrm{t\bar{c}e^+e^-}]$ contact interaction, described in Equation (1). Referring to the anomalous coupling formalism described in Reference [9], using the cross section expression of Equation (2), an exclusion region in the κ_{Z} *vs.* κ_γ plane is obtained, as displayed in Figure 5a. QCD and ISR corrections as well as flavour changing decays of the top quark through anomalous vertices are taken into account in the limits computation. Using the Born-level cross section of Equation (2), a corresponding exclusion region in the $\mathrm{BR}(\mathrm{t} \rightarrow \mathrm{Zq})$ *vs.* $\mathrm{BR}(\mathrm{t} \rightarrow \gamma\mathrm{q})$ plane is found, as shown in Figure 5b. The anomalous coupling formalism upper limits are summarised in Table 7.

In conclusion, no evidence for single top production at LEP is observed and possible new physics responsible for this process is constrained.

$<\sqrt{s}>$	(GeV)	188.6	191.6	195.5	199.6	201.8	204.8	206.6
$\sigma_{95}(m_{\mathrm{t}} = 170$ GeV)	(pb)	0.36	0.87	0.77	0.54	0.62	0.63	0.51
$\sigma_{95}(m_{\mathrm{t}} = 175$ GeV)	(pb)	0.22	0.73	0.67	0.45	0.56	0.51	0.39
$\sigma_{95}(m_{\mathrm{t}} = 180$ GeV)	(pb)	0.21	0.75	0.64	0.42	0.52	0.48	0.37

Table 5: Measured 95% confidence level upper limits, σ_{95}, on the total cross section for single top production as a function of the centre-of-mass energy. The limits are given for three assumptions on the top quark mass.

	Λ (TeV)		
	Vector coupling	Scalar coupling	Tensor coupling
$m_{\mathrm{t}} = 170$ GeV	0.76	0.65	1.24
$m_{\mathrm{t}} = 175$ GeV	0.75	0.65	1.24
$m_{\mathrm{t}} = 180$ GeV	0.70	0.60	1.16

Table 6: Measured 95% confidence level lower limits on the energy scale parameter Λ in TeV. Three different scenarios for the coupling constants are considered: vectorial ($V_{ij} = 1$, $S_{RR} = 0$, $T_{RR} = 0$), scalar ($V_{ij} = 0$, $S_{RR} = 1$, $T_{RR} = 0$) and tensorial ($V_{ij} = 0$, $S_{RR} = 0$, $T_{RR} = 1$). Limits are given for three values of the top quark mass.

m_{t} (GeV)	170	175	180
$\|\kappa_{\mathrm{Z}}\|$	0.38	0.37	0.43
$\|\kappa_{\gamma}\|$	0.43	0.43	0.49
BR($\mathrm{t} \to \mathrm{Zq}$)	13.6%	13.7%	17.0%
BR($\mathrm{t} \to \gamma\mathrm{q}$)	4.4%	4.1%	4.9%

Table 7: Measured 95% confidence level upper limits on the anomalous-coupling parameters κ_{Z} and κ_{γ} and on the FCNC top decay branching fractions. Limits are given for three values of the top quark mass.

References

[1] G. Eilam, J.L. Hewett and A. Soni, Phys. Rev. **D44** (1991) 1473; C.S. Huang, X.H. Wu and S.H. Zhu, Phys. Lett. **B452** (1999) 143.

[2] C.S. Li, R.J. Oakes and J.M. Yang, Phys. Rev. **D49** (1994) 293; R.S. Chivukula, E.H. Simmons and J. Terning, Phys. Lett. **B 331** (1994) 383; J.L. Lopez, D.V. Nanopoulos and R. Rangarajan, Phys. Rev. **D56** (1997) 3100.

[3] T.P. Cheng and M. Sher, Phys. Rev. **D35** (1987) 3484; B. Mukhopadhyaya and S. Nandi, Phys. Rev. Lett. **66** (1991) 285; W.S. Hou, Phys. Lett. **B 296** (1992) 179; L. Hall and S. Weinberg, Phys. Rev. Rapid Comm. **D48** (1993) R979; M. Luke and M.J. Savage, Phys. Lett. **B 307** (1993) 387; D. Atwood, L. Reina and A. Soni, Phys. Rev. **D55** (1997) 3156.

[4] V. Barger, M.S. Berger and R.J.N. Phillips, Phys. Rev. **D52** (1995) 1663; H. Georgi *et al.*, Phys. Rev. **D51** (1995) 3888; C.T. Hill, Phys. Lett. **B 345** (1995) 483; B. Holdom, Phys. Lett. **B 351** (1995) 279; J. Berger *et al.*, Phys. Rev. **D54** (1996) 3598; B.A. Arbuzov and M.Y. Osipov, Phys. Atom. Nucl. **62** (1999) 485.

[5] E. Boos *et al.*, Eur. Phys. J. **C21** (2001) 81; S. Bar-Shalom *et al.*, Phys. Rev. **D57** (1998) 2957; D. Atwood, L. Reina and A. Soni, Phys. Rev. **D53** (1996) 1199; M. Chemtob and G. Moreau, Phys. Rev. **D59** (1999) 116012; U. Mahanta and A. Ghosal, Phys. Rev. **D57** (1998) 1735.

[6] CDF Collaboration, F. Abe *et al.*, Phys. Rev. Lett. **80** (1998) 2525.

[7] ALEPH Collaboration, A. Heiter *et al.*, Preprint CERN-EP/2002-042 (2002); OPAL Collaboration, G. Abbiendi *et al.*, Phys. Lett. **B 521** (2001) 181.

[8] S. Bar-Shalom and J. Wudka, Phys. Rev. **D60** (1999) 094016.

[9] V.F. Obraztsov, S.R. Slabospitsky and O.P. Yushchenko, Phys. Lett. **B 426** (1998) 393.

[10] T. Han and J.L. Hewett, Phys. Rev. **D60** (1999) 074015.

[11] L.J. Reinders, H. Rubinstein and S. Yazaki, Phys. Rep. **127** (1985) 1.

[12] L3 Collaboration, B. Adeva *et al.*, Nucl. Inst. Meth. **A 289** (1990) 35; J. A. Bakken *et al.*, Nucl. Inst. Meth. **A 275** (1989) 81; O. Adriani *et al.*, Nucl. Inst. Meth. **A 302** (1991) 53; O. Adriani *et al.*, Phys. Rev. **236** (1993) 1; B. Adeva *et al.*, Nucl. Inst. Meth. **A**

323 (1992) 109; M. Chemarin *et al.*, Nucl. Inst. Meth. **A 349** (1994) 345; M. Acciarri *et al.*, Nucl. Inst. Meth. **A 351** (1994) 300; I.C. Brock *et al.*, Nucl. Instr. and Meth. **A 381** (1996) 236; A. Adam *et al.*, Nucl. Inst. Meth. **A 383** (1996) 342; G. Basti *et al.*, Nucl. Inst. Meth. **A 374** (1996) 293.

[13] PHYTHIA version 5,722 is used: T. Sjöstrand, Preprint CERN-TH/7112/93 (1993) , revised 1995; T. Sjöstrand, Comp. Phys. Comm. **82** (1994) 74.

[14] KK2f version 4.12 is used: S. Jadach, B.F.L. Ward and Z. Wąs, Comp. Phys. Comm. **130** (2000) 260.

[15] KORALW version 1.33 is used: M. Skrzypek *et al.*, Comp. Phys. Comm. **94** (1996) 216.

[16] KORALZ version 4.03 is used: S. Jadach, B.F.L. Ward and Z. Wąs, Comp. Phys. Comm. **79** (1994) 503.

[17] PHOJET version 1.05 is used: R. Engel, Z. Phys. **66** (1995) 203; R. Engel and J. Ranft, Phys. Rev. **D54** (1996) 4244.

[18] EXCALIBUR version 1.11 is used: F.A. Berends, R. Pittau and R. Kleiss, Comp. Phys. Comm. **85** (1995) 437.

[19] L. Cuénoud, Generator of Flavour Changing Neutral Currents, Diploma thesis, University of Lausanne, (1996).

[20] B. Andersson *et al.*, Phys. Rep. **97** (1983) 31.

[21] GEANT version 3.15 is used: R. Brun *et al.*, Preprint CERN-DD/EE/84-1 (1984) , revised 1987; H. Fesefeldt, Report RWTH Aachen PITHA 85/02 (1985).

[22] L3 Collaboration, M. Acciarri *et al.*, Phys. Lett. **B 411** (1997) 373.

[23] S. Catani *et al.*, Phys. Lett. **B 269** (1991) 432; S. Bethke *et al.*, Nucl. Phys. **B 370** (1992) 310.

[24] L. Lönnblad, C. Peterson and T. Rögnvaldsson, Nucl. Phys. **B 349** (1991) 675; C. Peterson *et al.*, Comp. Phys. Comm. **81** (1994) 185.

[25] V.F. Obraztsov, Nucl. Inst. Meth. **A 316** (1992) 388.

The L3 Collaboration:

P.Achard[21] O.Adriani[18] M.Aguilar-Benitez[25] J.Alcaraz[25,19] G.Alemanni[23] J.Allaby[19] A.Aloisio[29] M.G.Alviggi[29] H.Anderhub[47] V.P.Andreev[6,34] F.Anselmo[9] A.Arefiev[28] T.Azemoon[3] T.Aziz[10,19] P.Bagnaia[39] A.Bajo[25] G.Baksay[26] L.Baksay[26] S.V.Baldew[2] S.Banerjee[10] Sw.Banerjee[4] A.Barczyk[47,45] R.Barillère[19] P.Bartalini[23] M.Basile[9] N.Batalova[44] R.Battiston[33] A.Bay[23] F.Becattini[18] U.Becker[14] F.Behner[47] L.Bellucci[18] R.Berbeco[3] J.Berdugo[25] P.Berges[14] B.Bertucci[33] B.L.Betev[47] M.Biasini[33] M.Biglietti[29] A.Biland[47] J.J.Blaising[4] S.C.Blyth[35] G.J.Bobbink[2] A.Böhm[1] L.Boldizsar[13] B.Borgia[39] S.Bottai[18] D.Bourilkov[47] M.Bourquin[21] S.Braccini[21] J.G.Branson[41] F.Brochu[4] J.D.Burger[14] W.J.Burger[33] X.D.Cai[14] M.Capell[14] G.Cara Romeo[9] G.Carlino[29] A.Cartacci[18] J.Casaus[25] F.Cavallari[39] N.Cavallo[36] C.Cecchi[33] M.Cerrada[25] M.Chamizo[21] Y.H.Chang[49] M.Chemarin[24] A.Chen[49] G.Chen[7] G.M.Chen[7] H.F.Chen[22] H.S.Chen[7] G.Chiefari[29] L.Cifarelli[40] F.Cindolo[9] I.Clare[14] R.Clare[38] G.Coignet[4] N.Colino[25] S.Costantini[39] B.de la Cruz[25] S.Cucciarelli[33] J.A.van Dalen[31] R.de Asmundis[29] P.Déglon[21] J.Debreczeni[13] A.Degré[4] K.Dehmelt[26] K.Deiters[45] D.della Volpe[29] E.Delmeire[21] P.Denes[37] F.DeNotaristefani[39] A.De Salvo[47] M.Diemoz[39] M.Dierckxsens[2] C.Dionisi[39] M.Dittmar[47,19] A.Doria[29] M.T.Dova[11,♯] D.Duchesneau[4] B.Echenard[21] A.Eline[19] H.El Mamouni[24] A.Engler[35] F.J.Eppling[14] A.Ewers[1] P.Extermann[21] M.A.Falagan[25] S.Falciano[39] A.Favara[32] J.Fay[24] O.Fedin[34] M.Felcini[47] T.Ferguson[35] H.Fesefeldt[1] E.Fiandrini[33] J.H.Field[21] F.Filthaut[31] P.H.Fisher[14] W.Fisher[37] I.Fisk[41] G.Forconi[14] K.Freudenreich[47] C.Furetta[27] Yu.Galaktionov[28,14] S.N.Ganguli[10] P.Garcia-Abia[5,19] M.Gataullin[32] S.Gentile[39] S.Giagu[39] Z.F.Gong[22] G.Grenier[24] O.Grimm[47] M.W.Gruenewald[17] M.Guida[40] R.van Gulik[2] V.K.Gupta[37] A.Gurtu[10] L.J.Gutay[44] D.Haas[5] R.Sh.Hakobyan[31] D.Hatzifotiadou[9] T.Hebbeker[1] A.Hervé[19] J.Hirschfelder[35] H.Hofer[47] M.Hohlmann[26] G.Holzner[47] S.R.Hou[49] Y.Hu[31] B.N.Jin[7] L.W.Jones[3] P.de Jong[2] I.Josa-Mutuberría[25] D.Käfer[1] M.Kaur[15] M.N.Kienzle-Focacci[21] J.K.Kim[43] J.Kirkby[19] W.Kittel[31] A.Klimentov[14,28] A.C.König[31] M.Kopal[44] V.Koutsenko[14,28] M.Kräber[47] R.W.Kraemer[35] W.Krenz[1] A.Krüger[46] A.Kunin[14] P.Ladron de Guevara[25] I.Laktineh[24] G.Landi[18] M.Lebeau[19] A.Lebedev[14] P.Lebrun[24] P.Lecomte[47] P.Lecoq[19] P.Le Coultre[47] J.M.Le Goff[19] R.Leiste[46] M.Levtchenko[27] P.Levtchenko[34] C.Li[22] S.Likhoded[46] C.H.Lin[49] W.T.Lin[49] F.L.Linde[2] L.Lista[29] Z.A.Liu[7] W.Lohmann[46] E.Longo[39] Y.S.Lu[7] K.Lübelsmeyer[1] C.Luci[39] L.Luminari[39] W.Lustermann[47] W.G.Ma[22] L.Malgeri[21] A.Malinin[28] C.Maña[25] D.Mangeol[31] J.Mans[37] J.P.Martin[24] F.Marzano[39] K.Mazumdar[10] R.R.McNeil[6] S.Mele[19,29] L.Merola[29] M.Meschini[18] W.J.Metzger[31] A.Mihul[12] H.Milcent[19] G.Mirabelli[39] J.Mnich[1] G.B.Mohanty[10] G.S.Muanza[24] A.J.M.Muijs[2] B.Musicar[41] M.Musy[39] S.Nagy[16] S.Natale[21] M.Napolitano[29] F.Nessi-Tedaldi[47] H.Newman[32] T.Niessen[1] A.Nisati[39] H.Nowak[46] R.Ofierzynski[47] G.Organtini[39] C.Palomares[19] D.Pandoulas[1] P.Paolucci[29] R.Paramatti[39] G.Passaleva[18] S.Patricelli[29] T.Paul[11] M.Pauluzzi[33] C.Paus[14] F.Pauss[47] M.Pedace[39] S.Pensotti[27] D.Perret-Gallix[4] B.Petersen[31] D.Piccolo[29] F.Pierella[9] M.Pioppi[33] P.A.Piroué[37] E.Pistolesi[27] V.Plyaskin[28] M.Pohl[21] V.Pojidaev[18] J.Pothier[19] D.O.Prokofiev[44] D.Prokofiev[34] J.Quartieri[40] G.Rahal-Callot[47] M.A.Rahaman[10] P.Raics[16] N.Raja[10] R.Ramelli[47] P.G.Rancoita[27] R.Ranieri[18] A.Raspereza[46] P.Razis[30] D.Ren[47] M.Rescigno[39] S.Reucroft[11] S.Riemann[46] K.Riles[3] B.P.Roe[3] L.Romero[25] A.Rosca[8] S.Rosier-Lees[4] S.Roth[1] C.Rosenbleck[1] B.Roux[31] J.A.Rubio[19] G.Ruggiero[18] H.Rykaczewski[47] A.Sakharov[47] S.Saremi[6] S.Sarkar[39] J.Salicio[19] E.Sanchez[25] M.P.Sanders[31] C.Schäfer[19] V.Schegelsky[34] S.Schmidt-Kaerst[1] D.Schmitz[1] H.Schopper[48] D.J.Schotanus[31] G.Schwering[1] C.Sciacca[29] L.Servoli[33] S.Shevchenko[32] N.Shivarov[42] V.Shoutko[14] E.Shumilov[28] A.Shvorob[32] T.Siedenburg[1] D.Son[43] C.Souga[24] P.Spillantini[18] M.Steuer[14] D.P.Stickland[37] B.Stoyanov[42] A.Straessner[19] K.Sudhakar[10] G.Sultanov[42] L.Z.Sun[22] S.Sushkov[8] H.Suter[47] J.D.Swain[11] Z.Szillasi[26,¶] X.W.Tang[7] P.Tarjan[16] L.Tauscher[5] L.Taylor[11] B.Tellili[24] D.Teyssier[24] C.Timmermans[31] Samuel C.C.Ting[14] S.M.Ting[14] S.C.Tonwar[10,19] J.Tóth[13] C.Tully[37] K.L.Tung[7] J.Ulbricht[47] E.Valente[39] R.T.Van de Walle[31] R.Vasquez[44] V.Veszpremi[26] G.Vesztergombi[13] I.Vetlitsky[28] D.Vicinanza[40] G.Viertel[47] S.Villa[38] M.Vivargent[4] S.Vlachos[5] I.Vodopianov[34] H.Vogel[35] H.Vogt[46] I.Vorobiev[35,28] A.A.Vorobyov[34] M.Wadhwa[5] W.Wallraff[1] X.L.Wang[22] Z.M.Wang[22] M.Weber[1] P.Wienemann[1] H.Wilkens[31] S.Wynhoff[37] L.Xia[32] Z.Z.Xu[22] J.Yamamoto[3] B.Z.Yang[22] C.G.Yang[7] H.J.Yang[3] M.Yang[7] S.C.Yeh[50] An.Zalite[34] Yu.Zalite[34] Z.P.Zhang[22] J.Zhao[22] G.Y.Zhu[7] R.Y.Zhu[32] H.L.Zhuang[7] A.Zichichi[9,19,20] B.Zimmermann[47] M.Zöller[1]

1 I. Physikalisches Institut, RWTH, D-52056 Aachen, Germany[§]
III. Physikalisches Institut, RWTH, D-52056 Aachen, Germany[§]
2 National Institute for High Energy Physics, NIKHEF, and University of Amsterdam, NL-1009 DB Amsterdam, The Netherlands
3 University of Michigan, Ann Arbor, MI 48109, USA
4 Laboratoire d'Annecy-le-Vieux de Physique des Particules, LAPP,IN2P3-CNRS, BP 110, F-74941 Annecy-le-Vieux CEDEX, France
5 Institute of Physics, University of Basel, CH-4056 Basel, Switzerland
6 Louisiana State University, Baton Rouge, LA 70803, USA
7 Institute of High Energy Physics, IHEP, 100039 Beijing, China[△]
8 Humboldt University, D-10099 Berlin, Germany[§]
9 University of Bologna and INFN-Sezione di Bologna, I-40126 Bologna, Italy
10 Tata Institute of Fundamental Research, Mumbai (Bombay) 400 005, India
11 Northeastern University, Boston, MA 02115, USA
12 Institute of Atomic Physics and University of Bucharest, R-76900 Bucharest, Romania
13 Central Research Institute for Physics of the Hungarian Academy of Sciences, H-1525 Budapest 114, Hungary[‡]
14 Massachusetts Institute of Technology, Cambridge, MA 02139, USA
15 Panjab University, Chandigarh 160 014, India.
16 KLTE-ATOMKI, H-4010 Debrecen, Hungary[¶]
17 Department of Experimental Physics, University College Dublin, Belfield, Dublin 4, Ireland
18 INFN Sezione di Firenze and University of Florence, I-50125 Florence, Italy
19 European Laboratory for Particle Physics, CERN, CH-1211 Geneva 23, Switzerland
20 World Laboratory, FBLJA Project, CH-1211 Geneva 23, Switzerland
21 University of Geneva, CH-1211 Geneva 4, Switzerland
22 Chinese University of Science and Technology, USTC, Hefei, Anhui 230 029, China[△]
23 University of Lausanne, CH-1015 Lausanne, Switzerland
24 Institut de Physique Nucléaire de Lyon, IN2P3-CNRS,Université Claude Bernard, F-69622 Villeurbanne, France
25 Centro de Investigaciones Energéticas, Medioambientales y Tecnológicas, CIEMAT, E-28040 Madrid, Spain♭
26 Florida Institute of Technology, Melbourne, FL 32901, USA
27 INFN-Sezione di Milano, I-20133 Milan, Italy
28 Institute of Theoretical and Experimental Physics, ITEP, Moscow, Russia
29 INFN-Sezione di Napoli and University of Naples, I-80125 Naples, Italy
30 Department of Physics, University of Cyprus, Nicosia, Cyprus
31 University of Nijmegen and NIKHEF, NL-6525 ED Nijmegen, The Netherlands
32 California Institute of Technology, Pasadena, CA 91125, USA
33 INFN-Sezione di Perugia and Università Degli Studi di Perugia, I-06100 Perugia, Italy
34 Nuclear Physics Institute, St. Petersburg, Russia
35 Carnegie Mellon University, Pittsburgh, PA 15213, USA
36 INFN-Sezione di Napoli and University of Potenza, I-85100 Potenza, Italy
37 Princeton University, Princeton, NJ 08544, USA
38 University of Californa, Riverside, CA 92521, USA
39 INFN-Sezione di Roma and University of Rome, "La Sapienza", I-00185 Rome, Italy
40 University and INFN, Salerno, I-84100 Salerno, Italy
41 University of California, San Diego, CA 92093, USA
42 Bulgarian Academy of Sciences, Central Lab. of Mechatronics and Instrumentation, BU-1113 Sofia, Bulgaria
43 The Center for High Energy Physics, Kyungpook National University, 702-701 Taegu, Republic of Korea
44 Purdue University, West Lafayette, IN 47907, USA
45 Paul Scherrer Institut, PSI, CH-5232 Villigen, Switzerland
46 DESY, D-15738 Zeuthen, Germany
47 Eidgenössische Technische Hochschule, ETH Zürich, CH-8093 Zürich, Switzerland
48 University of Hamburg, D-22761 Hamburg, Germany
49 National Central University, Chung-Li, Taiwan, China
50 Department of Physics, National Tsing Hua University, Taiwan, China
§ Supported by the German Bundesministerium für Bildung, Wissenschaft, Forschung und Technologie
‡ Supported by the Hungarian OTKA fund under contract numbers T019181, F023259 and T037350.
¶ Also supported by the Hungarian OTKA fund under contract number T026178.
♭ Supported also by the Comisión Interministerial de Ciencia y Tecnología.
♯ Also supported by CONICET and Universidad Nacional de La Plata, CC 67, 1900 La Plata, Argentina.
△ Supported by the National Natural Science Foundation of China.

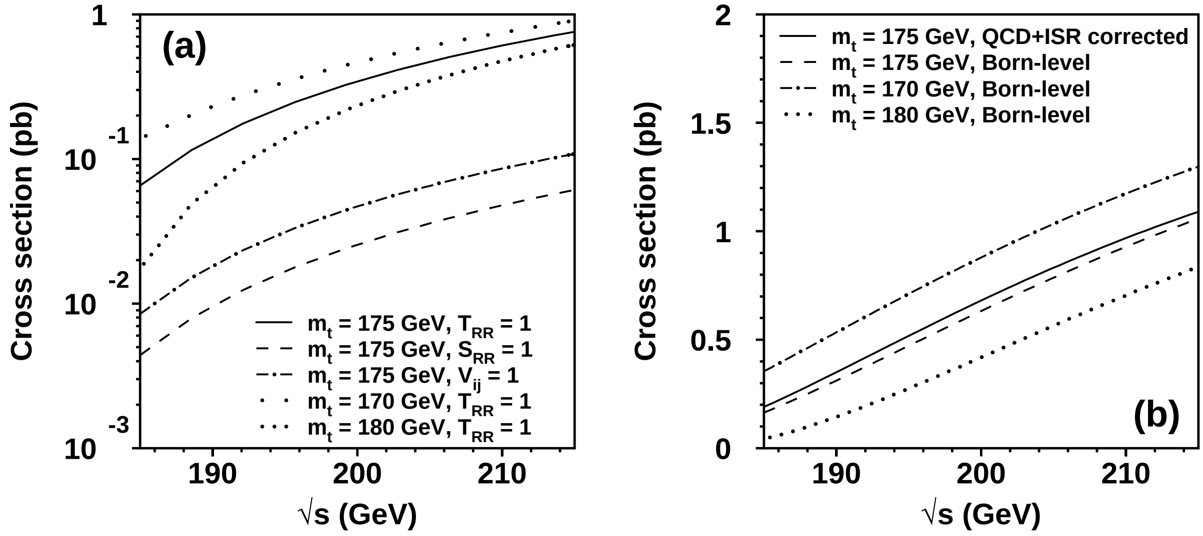

Figure 1: Theoretical total cross section for single top production as a function of the centre-of-mass energy for three different top quark mass values for (a) $[t\bar{c}e^+e^-]$ contact interactions with different assumptions on the Lorentz structure and an energy scale parameter $\Lambda = 1$ TeV and (b) the model described in Equation (2) where CDF limits on the values for the anomalous constants are assumed.

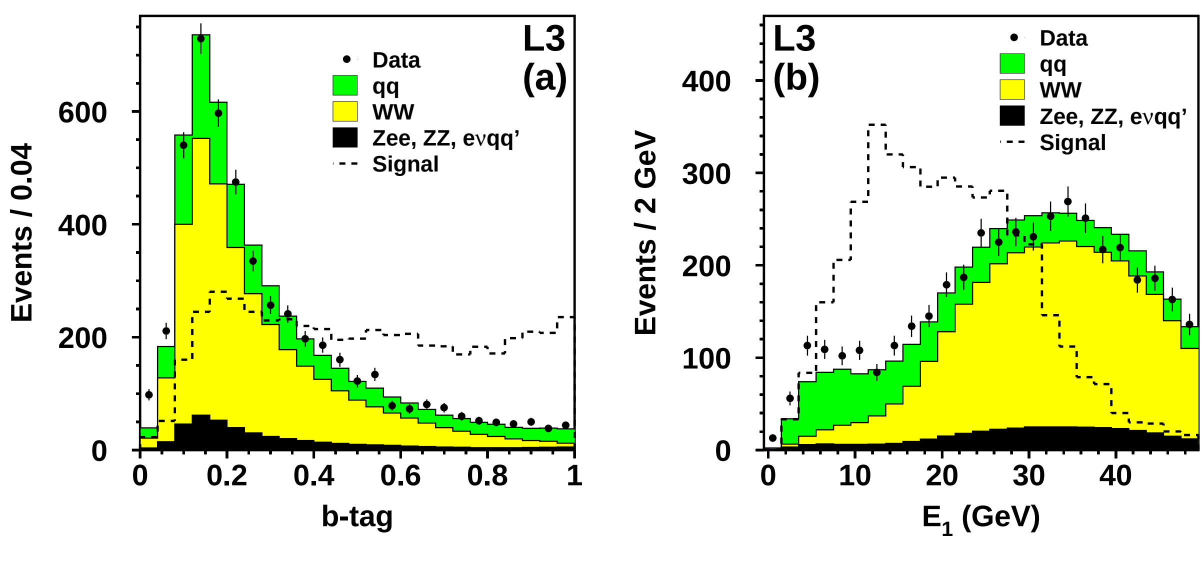

Figure 2: Distributions for the leptonic channel of (a) the b-tag discriminant variable for the most energetic jet, and (b) the energy E_1 of the least energetic jet. The signal histogram is for a top quark mass of 175 GeV and is normalised to the number of data events. Background expectations are also shown.

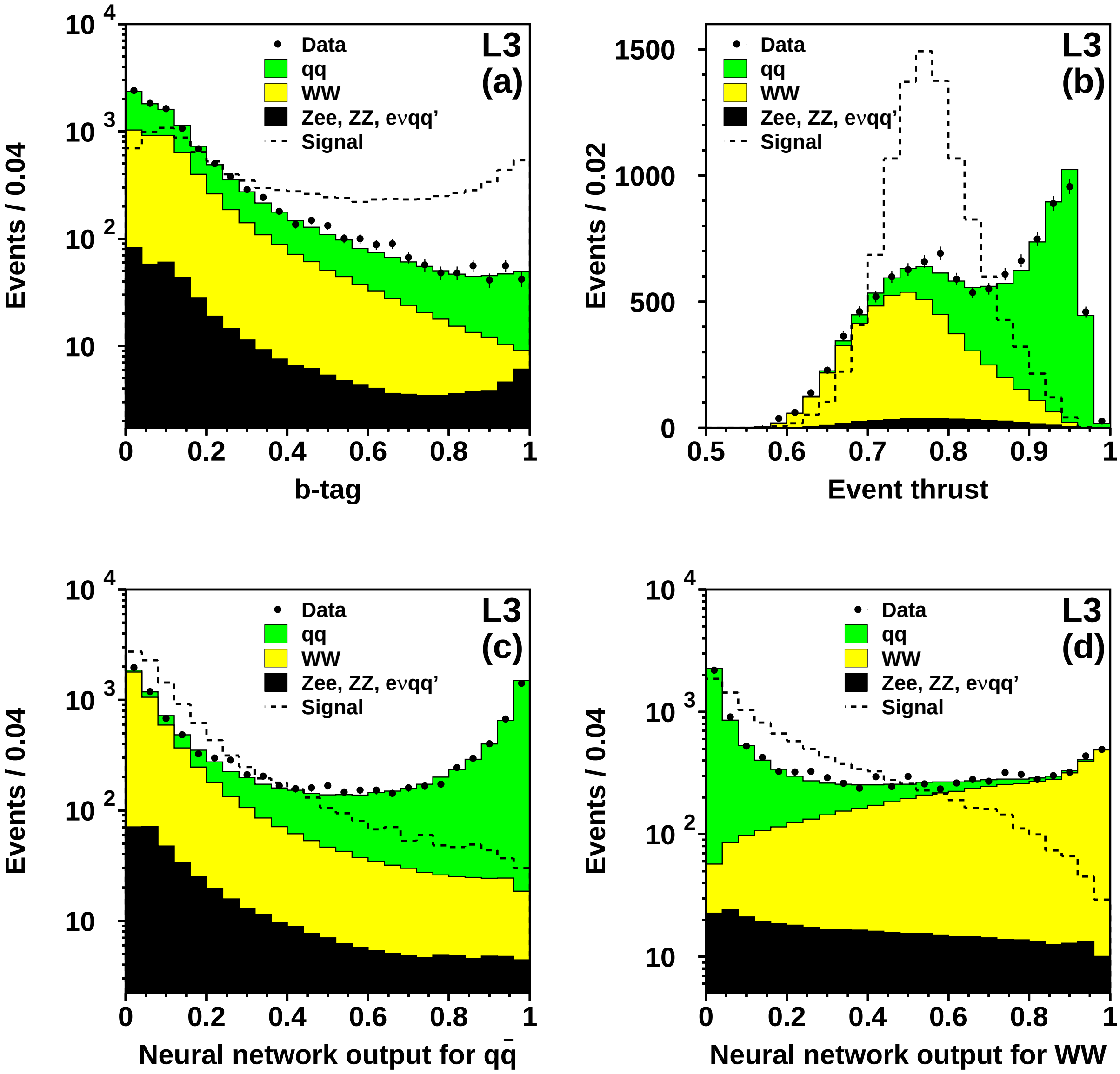

Figure 3: Distributions for the hadronic channel after preselection of (a) the b-tag variable of the b jet, (b) the event thrust and (c), (d) the neural network outputs related to $e^+e^- \rightarrow q\bar{q}(\gamma)$ and $e^+e^- \rightarrow W^+W^-$. The signal histogram is for a top quark mass of 175 GeV and is normalised to the number of data events. Background expectations are also shown.

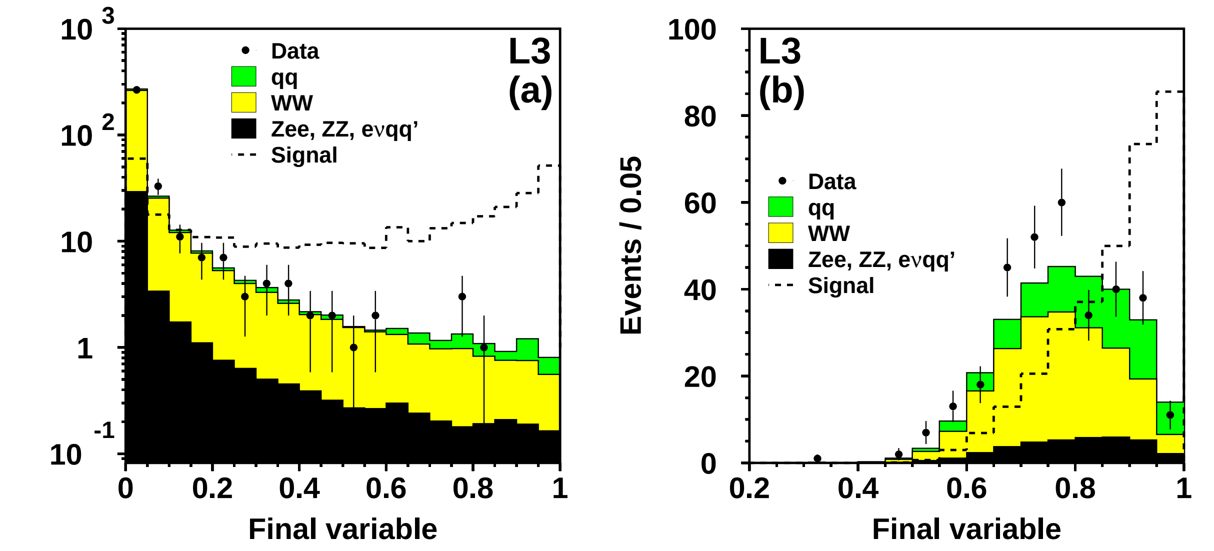

Figure 4: Distribution of the final discriminating variable for (a) the leptonic channel and (b) the hadronic channel. The signal histogram is for a top quark mass of 175 GeV and is normalised to the number of data events. Background expectations are also shown.

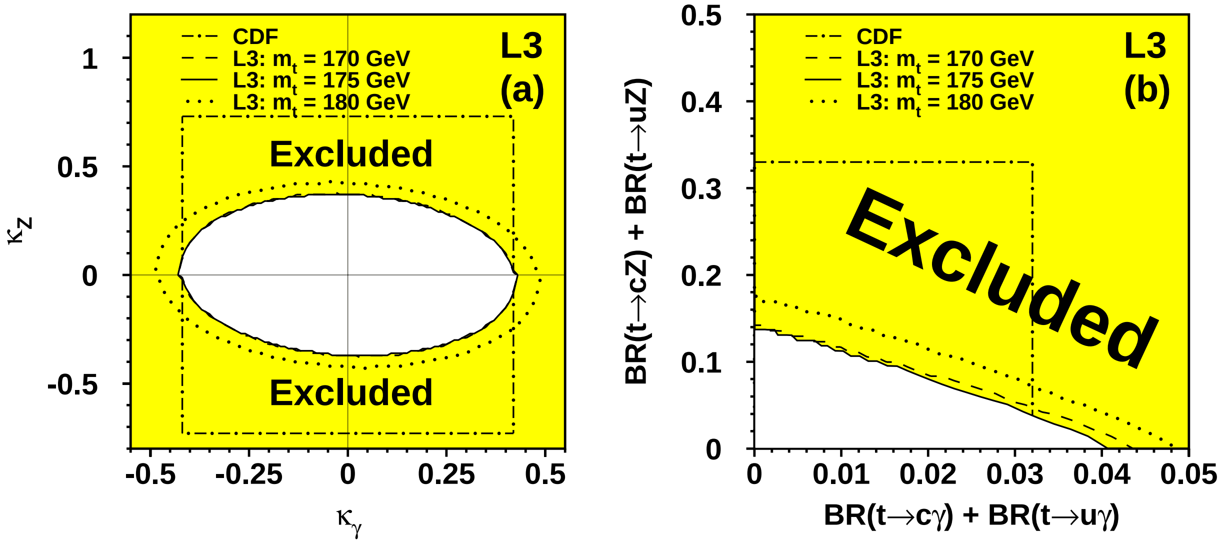

Figure 5: Exclusion regions at the 95% confidence level in (a) the κ_Z *vs.* κ_γ plane and (b) the BR(t $\to$ Zq) *vs.* BR(t $\to$ γq) plane for three different values of the top quark mass. The CDF exclusion domain is also shown. On Figure (a) the curves m_t = 170 GeV and m_t = 175 GeV are almost overlapping.